Solvation Structure, Thermodynamics, and Molecular Conformational Equilibria for *n*-Butane in Water Analyzed by Reference Interaction Site Model Theory Using an All-Atom Solute Model

Qizhi Cui and Vedene H. Smith, Jr.*

Department of Chemistry, Queen's University, Kingston, Ontario, Canada K7L 3N6

Received: January 18, 2002

For the four thermodynamic states: temperature $T = 283.15$, 298.15, 313.15, and 328.15 K and the corresponding bulk water density $\rho = 0.9997$, 0.9970, 0.9922, and 0.9875 g cm^{-3}, for which experimental data are available, we have studied hydration structure, hydration thermodynamics, and molecular conformational equilibria for *n*-butane in water at infinite dilution, by means of the hypernetted chain closure reference interaction site model (HNC−RISM) theory with an all-atom solute model. The hydration structures of the *trans* and the *gauche* conformers of *n*-butane are presented and analyzed at the atomic level in terms of the atomic solute−solvent radial distribution functions. With these radial distribution functions as input, the *n*-butane conformational average hydration free energies, energies, enthalpies, and entropies are calculated. At room temperature, the normalized equilibrium distribution of *n*-butane conformers, the water solvent-induced rotational free energy surface and the *trans*−*gauche* and *trans*−*cis* cavity thermodynamic properties are calculated. With the optimized nonbonded potential parameters based on the CHARMM96 all-atom model for alkanes (Yin, D.; Mackerell, A. D., Jr. *J. Comput. Chem.* **1998**, *19*, 334), *n*-butane hydration thermodynamics and its conformational equilibria in water are well described by the HNC−RISM theory in comparison with the available experimental and computer simulation results. We also calculated the solute density derivatives of the water−water radial distribution functions δh_{vv}, with the optimized CHARMM96 all-atom model, the united-atom OPLS (optimized potentials for liquid simulations), and the all-atom OPLS models for *n*-butane, respectively. The $\delta h_{vv}(r)$ reflect the effect of increased pressure disrupting the hydrogen bonding between water molecules. The all-atom model seems to enhance such an effect due to the well-documented shortcoming of the RISM theory in the treatment of the excluded volume of so-called auxiliary sites.

I. Introduction

Two important problems in the study of the aqueous solution behavior of biomolecules are the restructuring of water around the molecules and the solvent influence on the conformational structure of the molecules. Small flexible hydrocarbon molecules have been used as models for studying those problems.[1] Among them, *n*-butane, which has only one conformational degree of freedom, is perhaps the simplest molecule available for studying the two problems at the same time. *n*-butane has been studied extensively in the gas phase,[1−8] in the neat liquid,[9−17] and in apolar[15,18−23] and aqueous solutions.[15,16,23−33]

There are two kinds of models for representing the *n*-butane molecule. One is a united-atom model, namely that the methyl and methylene groups are approximately considered as one site of pair interactions, respectively. In this model, the hydrogens of the CH_n groups are implicitly treated, the interaction sites for the CH_n groups are centered on the carbons, and the CH_n groups are all taken as neutral. The other one is an all-atom model, namely that all atoms of the *n*-butane molecule are considered as the sites of pair interactions. In this model, the hydrogens of the CH_n groups are explicitly treated, each atom is assigned an atomic charge, and the CH_n groups need not be neutral.

In computer simulation studies,[16,17,23,26−29] both united-atom and all-atom solute models have been employed. Tobias and Brooks, III,'s simulation[23] indicated that the united-atom and the all-atom butane model may produce significantly different distributions of the *n*-butane conformers in solvents. They show that the *gauche* populations are essentially unchanged relative to the gas phase for the united-atom model, while they are significantly increased for the all-atom model, in both polar and apolar solvents. In analytic theoretical studies, rarely have all-atom models been employed. To the best of our knowledge, no analytic results for the molecular conformational equilibra of *n*-butane in water with an all-atom solute model have been reported so far. With the united-atom model, Pratt and coworkers[24,25,30,31] analyzed *n*-butane hydrophobic effects by means of integral equation theory and information theory (IT). The hypernetted chain closure reference interaction site model (HNC−RISM)[34−38] theory provides another powerful theoretical tool to characterize molecular liquids. It has been successfully used in the calculation of the structural and thermodynamic properties of various chemical and biological systems and solutions.[39] With the united-atom solute model, Zichi and Rossky employed HNC−RISM theory to study the molecular conformational equilibria for *n*-butane in apolar and polar liquids.[15]

The HNC−RISM approach provides a cost-efficient tool to describe microscopic molecular effects of an aqueous solvent. However, there are some shortcomings in this approach such as the imperfect treatment of the excluded volume of the so-called auxiliary sites, and no intramolecular correlation included

* Corresponding author. Fax: 1-613-533-6669. E-mail:vhsmith@chem.queensu.ca.

10.1021/jp020191n CCC: $22.00
Published on Web 06/05/2002

in the HNC closure.[32,33,40−47] Those shortcomings of the HNC−RISM theory result in rather poor predictions for the thermodynamics of hydrophobic hydration of neutral solutes such as hydrocarbons or rare gases. It overestimates the hydration free energy and gives the wrong dependence of the hydration free energy on the solute size.[40−43]

To improve the poor predictions, Lue and Blankschtein[41] employed the Martynov-Sarkisov (MaS) closure[48] or the more general Ballone-Pastore-Galli-Gazzillo (BPGG) closure[49] instead of the HNC closure and found that the RISM prediction for methane, ethane, and propane hydration thermodynamics can be substantially improved. However, both closures can be used only for nonpolar solute species, in the absence of Coulombic site−site interactions. Thus, these two closures cannot be used for all-atom solute models where site charges are involved.

Recently, Roux and co-workers[32] have made bridge corrections to the HNC closure for the three-dimensional HNC−RISM theory.[50−56] They introduced two empirical bridge functions for the water hydrogen and the water oxygen, respectively. The two bridge functions play the role of effective potentials and are adjusted empirically to improve the accuracy of the RISM theory. Kovalenko and Hirata[33] introduced a repulsive bridge correction (RBC) to the HNC closure for both one-dimensional and three-dimensional HNC−RISM theory. The RBC is intended to counter the overestimation of water ordering around a hydrophobic solute in the HNC−RISM approach and thus to refine the entropic component in the hydration free energy. But they employed only the united-atom representation for the *n*-butane molecule.

In our recent studies,[57,58] we have found that with the optimized nonbonded potential parameters based on CHARMM96 all-atom model for alkanes,[59] not only can the hydration structure of methane, ethane, and propane be analyzed at the atomic level but also the HNC−RISM prediction for the hydration thermodynamic properties can be much improved in the temperature range of interest (10−55 °C) in which experimental data are available.

In this paper, we employ such an all-atom model for the *n*-butane molecule to study its solvation structure, thermodynamics and conformational equilibria in water by means of the HNC−RISM theory. We choose four thermodynamic states: temperature $T = 283.15$, 298.15, 313.15, and 328.15 K and the corresponding bulk water density $\rho = 0.9997$, 0.9970, 0.9922, and 0.9875 g cm^{-3}. These are the only ones for which experimental data[60,61] are available. At these states, the atomic solute−solvent radial distribution functions and the corresponding running coordination numbers are obtained by means of the HNC−RISM theory. The hydration structures of the *trans* and the *gauche* conformers of *n*-butane are analyzed at the atomic level in terms of the atomic solute−solvent radial distribution functions. With the radial distribution functions as input, the normalized equilibrium distribution of *n*-butane conformers, the water solvent-induced rotational free energy surface, the *trans*−*gauche* cavity thermodynamic properties and the *trans*−*cis* cavity free energy are calculated. Finally, the conformational average hydration free energies, energies, enthalpies, and entropies are calculated and compared with experiments.

Hydrophobic hydration and the associated hydrophobic effect is still a controversial topic and there remains considerable debate about its molecular origin as indicated recently by experimentalists, Bowron et al.,[62] and theoreticians, Dill et al.[63] In particular, the changes in the hydrogen bonding structure of water in the vicinity of a nonpolar solute molecule are still not well understood and still debatable.

The fundamental model for water structure around a hydrophobic solute is the so-called iceberg model suggested by Frank and Evans in 1945.[64] This model has been supported by many theoretical,[24,39,65−67] computer simulation[67−81] and experimental[62,81−84] studies in which the hydrogen bonding network in water was analyzed in terms of the water−water radial distribution functions, the hydrogen bond coordination number, energy, and geometry. It has been believed that hydrophobic solutes increase the hydrogen bonding structure of water in the first hydration shell, even though the changes have been proved to be very small. However this usual belief is true only for small solute molecules in cold water (room temperature or below).

Solute size, shape, and temperature effects on hydrophobic solvation have been intensively studied by means of analytical theories,[85−89] computer simulation,[90−104] and experiment[105] especially in recent years. It has been shown that the mechanism of hydrophobic solvation depends on solute size, shape, and temperature.[63] For small solute molecules, water molecules in the first solvation shell exhibit enhanced structuring, but this structuring is decreased with increasing solute size, decreasing curvature, and increasing temperature. By means of Monte Carlo (MC) simulations with a simplified two dimensional model of water, the so-called Mercedes Benz (MB) model, Dill and coworkers[103,104] showed that a large spherical nonpolar solute (much larger than a water) will break the hydrogen bonds in the first hydration shell, and thus the water structure is decreased. They[106] also show that there is a temperature T_S at which the transfer entropy of nonpolar solutes into water is zero: below T_S, shell water molecules have more hydrogen bonds than bulk water molecules; above T_S, the reverse is true. Thus, a hydophobic surface always breaks the hydrogen bonds in the water near to the surface at all temperatures. This has been observed by Du et al.[105] in their surface vibrational spectroscopic studies. They found that for air−water and oil−water interfaces, the interface water layer is less ordered.

By means of MC simulations, with a united-atom model for *n*-butane, Jorgensen[26] found that the average number, strength, and angle for the hydrogen bonds is the same in all regions of the solution as for bulk water, even though he predicted slightly increased hydrogen bonding peak in comparison with pure water. By means of molecular dynamics (MD) simulations, with a united-atom model for ethane, Mancera and Buckingham[96] found that in the temperature range (279−352K), the average hydration bond coordination numbers of the hydration-shell molecules are consistently slightly smaller than that of the bulk molecules. By means of MD simulations, with united-atom models for methane and Lennard-Jones spheres, Chau et al.[97] found that using various definitions of hydrogen bonds, the average number of hydrogen bonds per water molecule in the solvation shell is always smaller than that in the bulk phase.

By means of HNC−RISM theory, Yu and Karplus[65] and Chong and Hirata[39,107] calculated the solute density derivatives of water−water radial distribution functions, δh_{vv} for ions, Lennard-Jones spheres, and water solute molecule in water and successfully analyzed the effects of increased solute density (or pressure for (N, T, V) ensemble) on the hydrogen bonding between water molecules. Using similar methods, in this work, we have calculated the δh_{vv} with the optimized CHARMM96 all-atom model for *n*-butane. For comparison, we also did the same calculations with the united-atom OPLS (optimized potentials for liquid simulations)[108] and the all-atom OPLS models[16] for *n*-butane, respectively.

In the next section we describe the theoretical methods used. In section III, the solvation structure, solvation thermodynamics and the molecular conformational equilibria for *n*-butane in water are analyzed. The concluding remarks are given in section IV.

II. Theoretical Methods

A. HNC−RISM Theory. More detailed formulas can be found in ref 57. Here we only give some main equations. At the infinite dilution limit, the solvent−solvent and solute−solvent RISM integral equation can be written in matrix form as[36−38]

$$\mathbf{h}^{vv} = \mathbf{w}^{v} * \mathbf{c}^{vv} * \mathbf{w}^{v} + \mathbf{w}^{v} * \mathbf{c}^{vv} * \rho_v \mathbf{h}^{vv} \quad (1)$$

$$\mathbf{h}^{uv} = \mathbf{w}^{u} * \mathbf{c}^{uv} * \mathbf{w}^{v} + \mathbf{w}^{u} * \mathbf{c}^{uv} * \rho_v \mathbf{h}^{vv} \quad (2)$$

where superscripts u and v denote solute and solvent, respectively. $\mathbf{h}^{vv}$ is the matrix of solvent−solvent intermolecular site−site total correlation functions, $\mathbf{c}^{vv}$ is the matrix of corresponding direct correlation functions, $\mathbf{w}^{v}$ is the solvent intramolecular correlation matrix, ρ_v is the number density of solvent molecules in the bulk, and * denotes a matrix convolution product. $\mathbf{h}^{uv}$ and $\mathbf{c}^{uv}$ are the corresponding matrixes for solute−solvent intermolecular correlation functions. $\mathbf{w}^{u}$ is the solute intramolecular correlation matrix. In Fourier k space, the elements of $\mathbf{w}^{v}$ or $\mathbf{w}^{u}$, $\bar{w}_{\alpha\lambda}(k) = (\sin(kL_{\alpha\lambda}))/(kL_{\alpha\lambda})$, where $L_{\alpha\lambda}$ is the distance between αth and λth sites in a solvent (v) or solute (u) molecule.

These equations can be solved sequentially with HNC-like closures. The solvent−solvent and solute−solvent potential energy between αth and λth sites is defined by

$$U_{\alpha\lambda} = 4\epsilon_{\alpha\lambda}\left[\left(\frac{\sigma_{\alpha\lambda}}{r}\right)^{12} - \left(\frac{\sigma_{\alpha\lambda}}{r}\right)^{6}\right] + \frac{Z_\alpha Z_\lambda}{r} \quad (3)$$

where $\sigma_{\alpha\lambda}$ and $\epsilon_{\alpha\lambda}$ are the Lennard-Jones distance and well depth parameters, respectively, calculated from the standard combination rule. Z_α and Z_λ are the site charges on the αth and λth sites, respectively.

With $\mathbf{h}^{vv}$ and $\mathbf{h}^{uv}$ as input, the isothermal solute density derivative of $\mathbf{h}^{vv}$ can be obtained

$$\delta\overline{\mathbf{h}^{vv}} = (\overline{\mathbf{w}^{v}} + \overline{\mathbf{h}^{vv}}\rho_v)\overline{\delta(c-\phi)^{vv}}(\rho_v\overline{\mathbf{h}^{vv}} + \overline{\mathbf{w}^{v}}) + \overline{\mathbf{h}^{vu}}\,\overline{\mathbf{w}^{u^{-1}}}\,\overline{\mathbf{h}^{uv}} \quad (4)$$

where the bar denotes functions in Fourier k space and ϕ is the solvent−solvent long range Coulombic potential.

The solvation structure at the atomic level can be measured from the radial distribution functions $g_{\alpha_u\lambda_v}(r) = h_{\alpha_u\lambda_v}(r) + 1$, which can be obtained from scattering experiments, and the corresponding running coordination numbers

$$N_{\alpha_u\lambda_v}(r) = \rho_{\lambda_v}\int_0^r dr' 4\pi r'^2 g_{\alpha_u\lambda_v}(r') \quad (5)$$

where ρ_{λ_v} is the number density of the λth site on solvent molecule v in the bulk.

The solvation thermodynamic quantities can be calculated from the site−site correlation functions.[65,109,110] At the infinite dilution limit, the solvation free energy per solute molecule,

$$\beta\Delta\mu = \rho_v \sum_{\alpha=1}^{n_u}\sum_{\lambda=1}^{n_v}\int 4\pi r^2\, dr\left[\frac{1}{2}h_{\alpha\lambda}^2(r) - c_{\alpha\lambda}(r) - \frac{1}{2}h_{\alpha\lambda}(r)c_{\alpha\lambda}(r)\right] \quad (6)$$

where n_u, n_v are the number of sites on solute u and solvent v, respectively.

The solvation energy per solute molecule,

$$\Delta\epsilon = \rho_v \sum_{\alpha=1}^{n_u}\sum_{\gamma=1}^{n_v}\int 4\pi r^2 dr U_{\alpha\gamma}(r) g_{\alpha\gamma}(r) + \frac{\rho_v^2}{2}\sum_{\lambda=1}^{n_v}\sum_{\gamma=1}^{n_v}\int 4\pi r^2\, dr U_{\lambda\gamma}(r)\delta h_{\lambda\gamma}(r) \quad (7)$$

The solvation entropy per solute molecule,

$$T\Delta s = \Delta\epsilon - \Delta\mu \quad (8)$$

To compare our computations with experiments, we convert the thermodynamic properties for the canonical ensemble (N, T, V) to those for the isothermal−isobaric ensemble (N, T, P) with the following thermodynamic relations. N, T, V and P are the number of molecules, temperature, volume and pressure, respectively.

At infinite dilution,[110]

$$T(\Delta s_P - \Delta s) = \Delta h - \Delta\epsilon = T\rho_v\alpha_{v,P}\left(\frac{\partial\Delta\mu}{\partial\rho_v}\right)_T \quad (9)$$

and[111]

$$\left(\frac{\partial\Delta\mu}{\partial\rho_v}\right)_T = \frac{1}{\rho_v^2\kappa_T} \quad (10)$$

where Δs_P is the solvation entropy per solute molecule at constant T and P, Δh is the solvation enthalpy, $\alpha_{v,P}$ is the isobaric thermal expansion coefficient of the pure solvent, and κ_T is the isothermal compressibility of the pure solvent. The values of $\alpha_{v,P}$ and κ_T can be found in ref 112.

B. Molecular Conformational Equilibria. For a solute with a single internal degree of freedom ϕ representing internal rotation, the normalized equilibrium distribution of conformers $S(\phi)$ is defined by[15]

$$S(\phi) = e^{-\beta W(\phi)}/\int_0^{2\pi} e^{-\beta W(\phi)}\, d\phi \quad (11)$$

where $\beta^{-1} = k_B T$ is the product of Boltzmann's constant k_B and the absolute temperature T, and $W(\phi)$ is the reversible work required to rotate the solute to the dihedral angle ϕ from the reference conformer, ϕ_0. In this paper, ϕ is the C−C−C−C dihedral angle of *n*-butane and measured relative to the *cis* conformer. ϕ_0 is chosen to be the *trans* conformer (i.e., $\phi_0 = \pi$).

$W(\phi)$ can be decomposed into two distinct contributions, the gas-phase rotational potential energy $V_0(\phi)$ and the free energy, $W_c(\phi)$, associated with the solute perturbation of the solvent structure.

$$W(\phi) = V_0(\phi) + W_c(\phi) \quad (12)$$

The revised Scott-Scheraga potential[19] is used for $V_0(\phi)$,

$$V_0(\phi) = 2.216 - 2.904\cos\phi - 3.134\cos^2\phi + 0.731\cos^3\phi + 6.268\cos^4\phi + 7.523\cos^5\phi \quad (13)$$

where $V_0(\phi)$ is measured in kcal/mol.

$W_c(\phi)$ is precisely the solvent induced reversible work required to rotate from ϕ_0 to ϕ in the solvent, or the cavity free energy.[113] It can be decomposed into the cavity energy $E_c(\phi)$

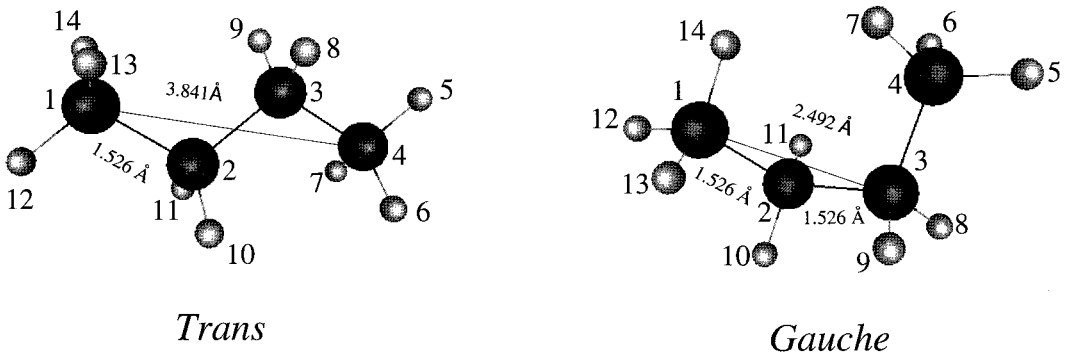

Figure 1. Molecular structures for *n*-butane comformers. The dark spheres (labeled 1, 2, 3, and 4) are carbon atoms, and the gray spheres are hydrogen atoms.

and entropy, $TS_c(\phi)$, contributions. For the chosen reference conformation, $W_c(\phi)$ and $E_c(\phi)$ can be written, respectively, as

$$W_c(\phi) = \Delta\mu(\phi) - \Delta\mu(\pi) \tag{14}$$

and

$$E_c(\phi) = \Delta\epsilon(\phi) - \Delta\epsilon(\pi) \tag{15}$$

where $\Delta\mu(\phi)$ and $\Delta\epsilon(\phi)$ are the solvation free energy and energy at constant temperature and solvent activity for a single fixed ϕ conformer in the solvent, respectively. They can be computed from either computer simulations or integral equation theories. In this work, we employ the HNC−RISM integral equation theory to calculate $\Delta\mu(\phi)$ and $\Delta\epsilon(\phi)$.

To obtain a quantitative measure of solvent-induced conformational shifts, we compare equilibrium constants K, defined by[114]

$$K = x_g/x_t = 2\int_0^{2\pi/3} S(\phi)\, d\phi / \int_{2\pi/3}^{4\pi/3} S(\phi)\, d\phi \tag{16}$$

for the *trans*−*gauche* isomerization in the gas and the water phases.

To compare with experiments, we calculate the conformational average solvation free energy per solute molecule,

$$\Delta\mu = \int_0^{2\pi} S(\phi)\Delta\mu(\phi)\, d\phi \tag{17}$$

and the conformational average solvation energy per solute molecule,

$$\Delta\epsilon = \int_0^{2\pi} S(\phi)\Delta\epsilon(\phi)\, d\phi \tag{18}$$

C. Parameters and Computation Procedures. In this work, the TIP3P water model[115] is employed for the solvent molecule and the all-atom *n*-butane model is employed for the solute molecule. For the carbons and the hydrogens of *n*-butane, the Lennard-Jones potential parameter ϵ's and σ's are taken from ref 58, which are optimized based on the CHARMM96 all-atom model for alkanes,[59] and the atomic charge Z's are adjusted to reproduce the experimental hydration free energy at 25 °C. The potential parameters used are summarized in Table 1. The molecular geometry parameters for *n*-butane with a fixed dihedral angle ϕ and the water molecule model are summarized in Table 2.

The dihedral angle ϕ is varied in increments of 5° from the *cis* ($\phi = 0°$) to the *trans* conformation ($\phi = 180°$). For each *n*-butane conformer, we employ the HNC−RISM theory to obtain the atomic solute−solvent radial distribution functions, $g_{\alpha_u\lambda_v}(r)$. With these functions as input, we calculate the corresponding running coordination numbers $N_{\alpha_u\lambda_v}(r)$ and the hydration thermodynamic properties as the function of ϕ: $\Delta\mu(\phi)$ and $\Delta\epsilon(\phi)$. Then, with the $\Delta\mu(\phi)$ as input, we calculate the molecular conformational equilibrium properties: $S(\phi)$, $W_c(\phi)$, and K. Finally, we calculate the *trans*−*gauche* cavity thermodynamic properties: $W_c(\pi/3)$, $E_c(\pi/3)$, and $TS_c(\pi/3)$, the *trans*−*cis* cavity free energy $W_c(0)$ and the conformational average solvation thermodynamic quantities: $\Delta\mu$, $\Delta\epsilon$, $T\Delta s$, Δh, and $T\Delta s_p$.

TABLE 1: Nonbonded Potential Parameters

molecule	atom	ϵ (kcal/mol)	σ (Å)	Z (e)
H_2O[a]	O	0.152	3.15	−0.834
	H	0.046	0.4	0.417
C_4H_{10}	(CH_3) C	0.078[b]	2.001[b]	−0.249
	(CH_3) H	0.024[b]	0.835[b]	0.066
	(CH_2) C	0.056[b]	2.001[b]	−0.121
	(CH_2) H	0.028[b]	0.835[b]	0.086

[a] Reference 115. [b] References 58 and 59.

TABLE 2: Geometric Parameters of Structures for Solvent and Solute Molecules

molecule	bond length (Å)	bond angle (deg)
H_2O[a]	O−H, 0.9572	H−O−H, 104.5
C_4H_{10}[b]	C−H, 1.09	H−C−H, 109.5
	C−C, 1.526	C−C−H, 109.5
		C−C−C, 109.5

[a] Reference 115. [b] Reference 122.

III. Results and Discussion

A. Solvation Structure. Since the solvation structures differ only slightly from each other in the temperature range in which we are interested, we only present our results for the solvation structures at room temperature $T = 298.15$ K and the bulk water density $\rho_v = 0.03333$ molecules/Å^3 (or 0.9970 g cm^{-3}).

To analyze the *n*-butane hydration structure at the atomic level, we label each atom of *n*-butane with a number. The molecular structure models for the *trans* and the *gauche* comformers are shown in Figure 1. Due to the molecular symmetry, there are only five distinguishable atomic sites (e.g., carbons 1 and 2, hydrogens 5, 6, and 8) for the *trans* conformer and seven distinguishable atomic sites (e.g., carbons 1 and 2, hydrogens 5, 6, 7, 8, and 9) for the *gauche* conformer. The radial distribution functions $g_{uv}(r)$ corresponding to these sites in water are shown in Figures 2−4. The main peak positions and the corresponding peak heights are listed in Tables 3 and 4, respectively.

TABLE 3: $g_{\alpha_u\lambda_v}(r)$ at the First Three Peak Positions (in Ångstroms) for the Methyl Group of the *trans* and the *gauche n*-Butane in Water

peaks	conformer	r, g_{C^1O}	r, g_{C^1H}	r, g_{H^5O}	r, g_{H^6O}	r, g_{H^7O}
first	*trans*	2.5, 1.66	1.0, 5.58	2.0, 1.20	1.9, 1.16	1.9, 1.16
	gauche	2.5, 1.68	1.0, 5.58	2.0, 1.16	2.0, 1.16	2.0, 1.08
second	*trans*	3.9, 1.00	3.2, 1.20	3.4, 0.95	3.5, 0.93	3.5, 0.93
	gauche	4.3, 0.99	3.2, 1.11	3.3, 0.93	3.4, 0.86	3.5, 0.88
third	*trans*	6.2, 1.04	6.0, 1.02	4.7, 1.00	4.7, 1.04	4.7, 1.04
	gauche	5.2, 1.05	5.4, 1.04	5.8, 1.02	4.8, 1.07	4.8, 1.12

TABLE 4: $g_{\alpha_u\lambda_v}(r)$ at the First Three Peak Positions (in Ångstroms) for the Methylene Group of the *trans* and the *gauche n*-Butane in Water

peaks	conformer	r, g_{C^2O}	r, g_{H^8O}	r, g_{H^8H}
first	*trans*	2.6, 1.21	1.9, 1.24	2.0, 1.00
	gauche	2.6, 1.22	1.9, 1.14	2.1, 0.93
second	*trans*	3.9, 1.14	3.5, 0.84	4.9, 1.07
	gauche	3.9, 1.12	3.4, 0.90	
third	*trans*	6.7, 1.02	4.7, 1.12	
	gauche	6.7, 1.02	4.5, 1.03	

The water structure around the methyl and methylene carbons of *n*-butane in the *trans* and the *gauche* conformations are shown in Figure 2a,b, respectively. From Figure 2a, we can see that the water structure around the methyl carbon is different for different conformers. Water molecules are more structured around the methyl carbon in the *trans* conformation than in the *gauche* conformation. But, for both conformers, the first peak of $g_{C^1O}(r)$ occurs at 2.5 Å which gives the closest distance for a water oxygen to approach the methyl carbon. Noticing that the sum of the first peak position of $g_{C^1O}(r)$ and the distance between two *trans* methyl carbons (R_{14} =3.841 Å) is 6.3 Å, we can assign the third peak of the *trans* $g_{C^1O}(r)$ at 6.2 Å to the closest distances for a water oxygen to approach the *trans* methyl carbon from the side of the other methyl carbon.

Since the space positions of the methylene carbons are not changed in the two conformations, $g_{C^2O}(r)$ and $g_{C^2H}(r)$ are not changed for the two conformers as shown in Figure 2(b). $g_{C^2O}(r)$ have two significant peaks at 2.6 and 3.9 Å, respectively. The first peak gives the closest distance for a water oxygen to approach the methylene carbon. Noticing that the sum of the first peak position of $g_{C^2O}(r)$ or $g_{C^1O}(r)$ and the carbon−carbon bond length (1.526 Å) is about 4.0 Å, we can assign the second peak of *trans* $g_{C^1O}(r)$ at 3.9 Å to the closest distances for a water oxygen to approach *trans* methyl carbon 1 from the side of its neighbor methylene carbon, and assign the second peak of $g_{C^2O}(r)$ at 3.9 Å to the closest distances for a water oxygen to approach methylene carbon 2 from the side of its neighbor methyl carbon and the side of the other methylene carbon, respectively.

Changed from the *trans* to the *gauche* conformation, the second peak of $g_{C^1O}(r)$ becomes flat and a third small peak occurs at 5.2 Å. Noticing that the sum of the first peak position of $g_{C^2O}(r)$ and the *gauche* carbon−carbon distance (R_{13} =2.492 Å) is about 5.1 Å, we can assign the third peak of the *gauche*

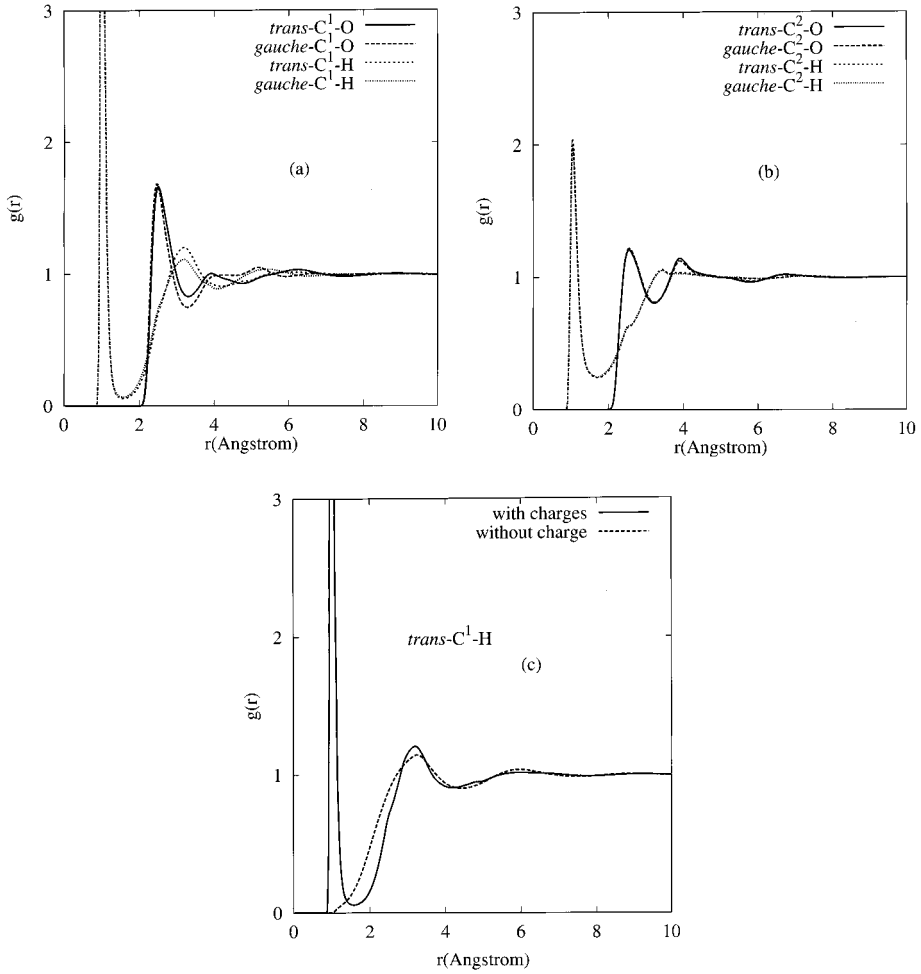

Figure 2. Radial distribution functions for the carbon atoms of *n*-butane in water at T = 298.15 K and ρ_v = 0.03333 molecules/Å^3. (a) $g_{C^1O}(r)$ and $g_{C^1H}(r)$ for the *trans* and the *gauche* methyl carbon 1, (b) $g_{C^2O}(r)$ and $g_{C^2H}(r)$ for the *trans* and the *gauche* methylene carbon 2, (c) $g_{C^1H}(r)$ for the *trans* methyl carbon 1 with and without site charges on atoms of the *n*-butane.

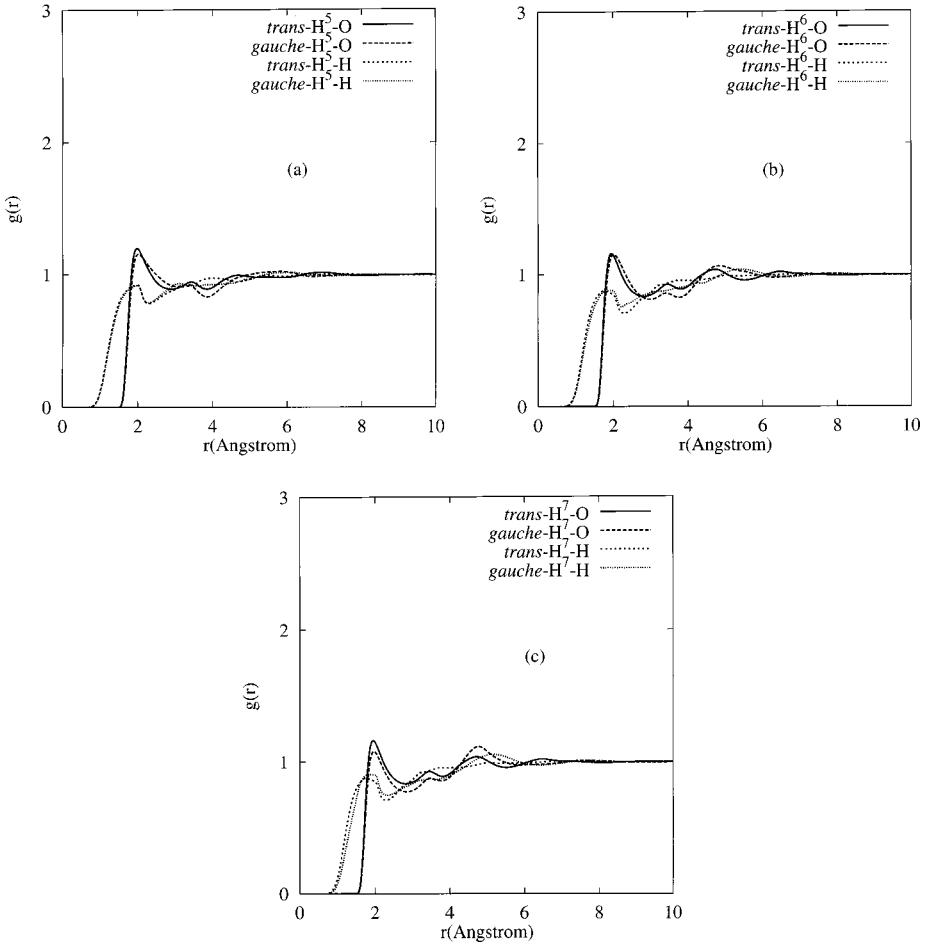

Figure 3. Radial distribution functions for the methyl hydrogen atoms of *n*-butane in the *trans* and the *gauche* conformations in water at $T = 298.15$ K and $\rho_v = 0.03333$ molecules/Å^3. (a) $g_{H^5O}(r)$ and $g_{H^5H}(r)$ for hydrogen 5, (b) $g_{H^6O}(r)$ and $g_{H^6H}(r)$ for hydrogen 6, (c) $g_{H^7O}(r)$ and $g_{H^7H}(r)$ for hydrogen 7.

$g_{C^1O}(r)$ at 5.2 Å to the closest distance for a water oxygen to appoach methyl carbon 1 from the side of methylene carbon 3 in the *gauche* conformation. As shown in Figure 1, in the *gauche* conformation methylene carbons become more exposed to water, which increases the chances for water molecules to approach methyl carbon 1 from the side of methylene carbon 3 and relatively decrease the chances for water molecules to approach methyl carbon 1 from the side of its neighbor methylene carbon 2. Therefore, the *gauche* $g_{C^1O}(r)$ shows a flat second peak around 4.0 Å and a distinct third peak around 5.0 Å. On the other hand, the *trans* $g_{C^1O}(r)$ has no distinct peak around 5.0 Å because in the *trans* conformation, methyl carbon 4 blocks the approach of a water molecule to the methyl carbon 1 from the side of methylene carbon 3.

In Figure 2, both the *trans* and the *gauche* $g_{CH}(r)$ have three peaks. The sharp peaks of $g_{C^1H}(r)$ and $g_{C^2H}(r)$ occurred at about 1.0 Å before the first peaks of $g_{C^1O}(r)$ and $g_{C^2O}(r)$ are unanticipated. Physically, those sharp peaks directly result from the Coulombic attraction between the butane carbons and water hydrogens. The peak position and height are sensitive to the Lennard-Jones parameter σ and the atomic site charge *Z*.

To see the origin of the sharp peak, we removed the charge on each site on butane to do the same calculations for the *trans* conformer and the obtained $g_{C^1H}(r)$ is shown in Figure 2c. One can see that, without site charges, and therefore no Coulombic attraction, the original first sharp peak of $g_{C^1H}(r)$ completely disappeared but the other features of the curve remain almost the same. The $g_{C^1H}(r)$ without site charges gives information about the molecular packing arrangements. It indicates that the steric constraints of the water molecular geometry do not allow the water hydrogen atom to approach the butane carbon so close as the sharp peak position. Therefore, the sharp peak cannot be used to estimate the closest distances for a water hydrogen to approach the methyl carbon and methylene carbon atoms of butane. However, this is contrary to the physical meaning of a radial distribution function. This contradiction reflects some shortcomings in the HNC−RISM theory, such as the imperfect treatment of the excluded volume of the so-called auxiliary sites and no intramolecular bond constraints in the HNC closure.[44,58] When polar electrostatic forces are dominant in determining the orientational structure present in fluids, the HNC−RISM theory may predict quantitatively less reliable results. But the qualitative features predicted by the theory are uniformly reliable.[36,37]

The second and the third peaks of the *trans* $g_{C^1H}(r)$ at 3.2 and 6.0 Å will give the closest distance and the next to the closest distance for a water hydrogen to approach the methyl carbon in the *trans* conformation, respectively. Changed from the *trans* to the *gauche* conformation, the height of the second peak of $g_{C^1H}(r)$ is decreased and the third peak is shifted to small *r*.

In Figure 2b, $g_{C^2H}(r)$ becomes flat starting from about 3.4 Å. It indicates that water hydrogens are randomly around the methylene carbons of *n*-butane and the closest distance for water hydrogens to approach the methylene carbons is about 3.4 Å.

Comparison of Figure 2a and Figure 2b shows that water is more structured around the methyl carbons than around the methylene carbons. Changed from the *trans* to the *gauche* conformation, the water structure around the methyl carbons

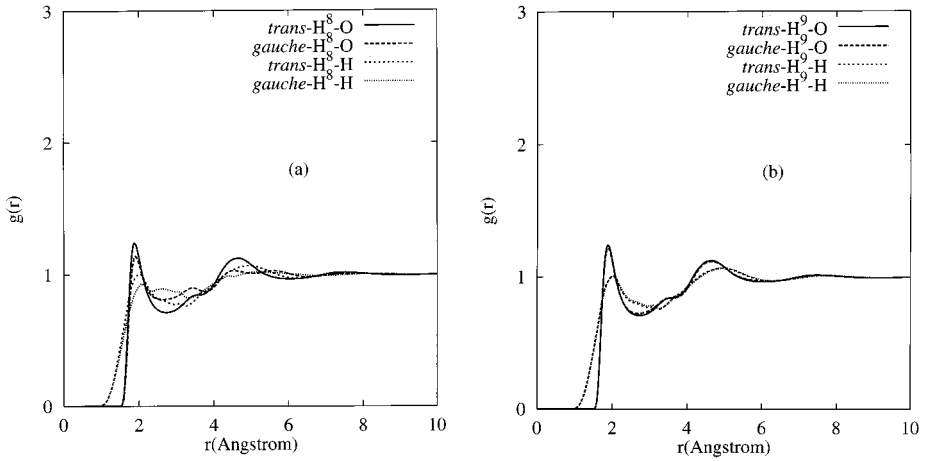

Figure 4. Radial distribution functions for the methylene hydrogen atoms of *n*-butane in the *trans* and the *gauche* conformations in water at $T = 298.15$ K and $\rho_v = 0.03333$ molecules/Å^3. (a) $g_{H^8O}(r)$ and $g_{H^8H}(r)$ for hydrogen 8; (b) $g_{H^9O}(r)$ and $g_{H^9H}(r)$ for hydrogen 9.

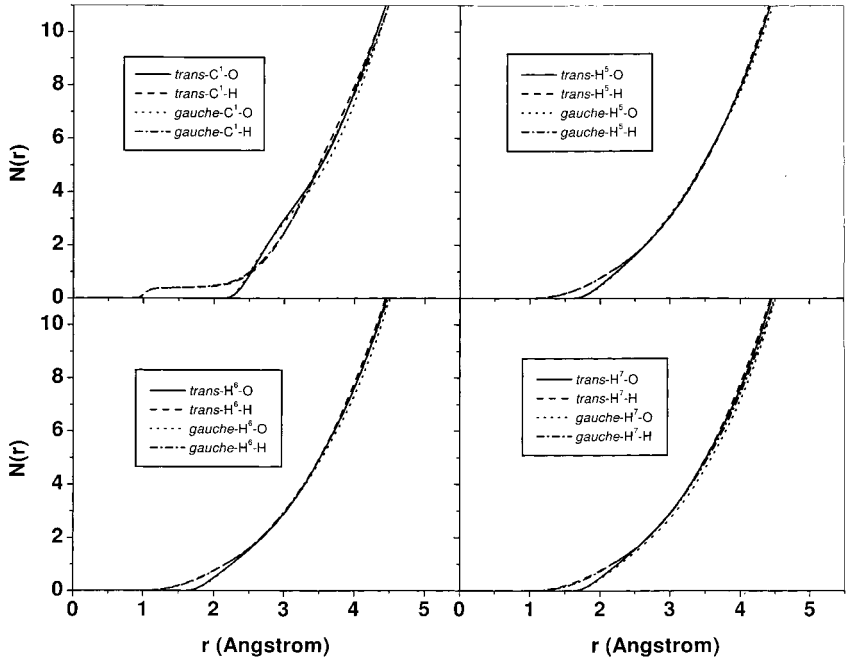

Figure 5. Running coordination numbers $N(r)$ for the *trans* and the *gauche* methyl group of *n*-butane in water.

changes significantly but remains the same around the methylene carbons.

The water structures around the methyl hydrogens in the *trans* and the *gauche* conformations are shown in Figure 3. There are two distinct hydration structures for the *trans* conformer and three distinct structures for the *gauche* conformer. Water oxygens are more orderly around the methyl hydrogens than water hydrogens and are more sensitive to the conformational change.

The water structures around the methylene hydrogens in the *trans* and the *gauche* conformations are shown in Figure 4. From Figure 4a, we can see that the water structure around the hydrogen 8 are significantly different for the two conformers. It is more ordered in the *trans* conformation than that in the *gauche* conformation. From Figure 4b, however, we can see that the water structure around hydrogen 9 is same for the two conformers. This is because methylene hydrogen 8 of the *trans* conformer and methylene hydrogen 9 of the *gauche* conformer are the same in their space positions.

In summary, the water structure around the different conformers are different. The water is more structured around the *trans* conformer than around the *gauche* conformer. For a fixed conformer, the water is more structured around the methyl carbons than around the methylene carbons. This is consistent with previous findings by means of integral equation theory[24] and simulations.[23,26]

The running coordination numbers $N_{\alpha_u\lambda_v}(r)$ for the methyl group and the methylene group of two *n*-butane conformers in water are shown in Figures 5 and 6, respectively. At small r, they have different behavior due to the solvation structure. At large r, they approach the same behavior. For different conformers, the corresponding $N_{\alpha_u\lambda_v}(r)$ show slightly different behavior. The average number of water oxygens in the first solvation shell can be estimated by integrating $g_{C^1O}(r)$ out to its first minimum (3.3 Å) and integrating $g_{C^2O}(r)$ out to its first minimum (3.2 Å), and is found to be 14.4. To compare with Jorgensen's Monte Carlo simulation results,[26] we calculate the coordination numbers $N_{C^1O}(5.3\text{ Å}) = 19$ and $N_{C^2O}(5.9\text{ Å}) = 27$, which match 17 and 25, repectively, given by Jorgensen's simulation using the united-atom *n*-butane model.

B. Solute Density Derivatives of Water−Water Radial Distribution Functions. In Figure 7 are shown the radial

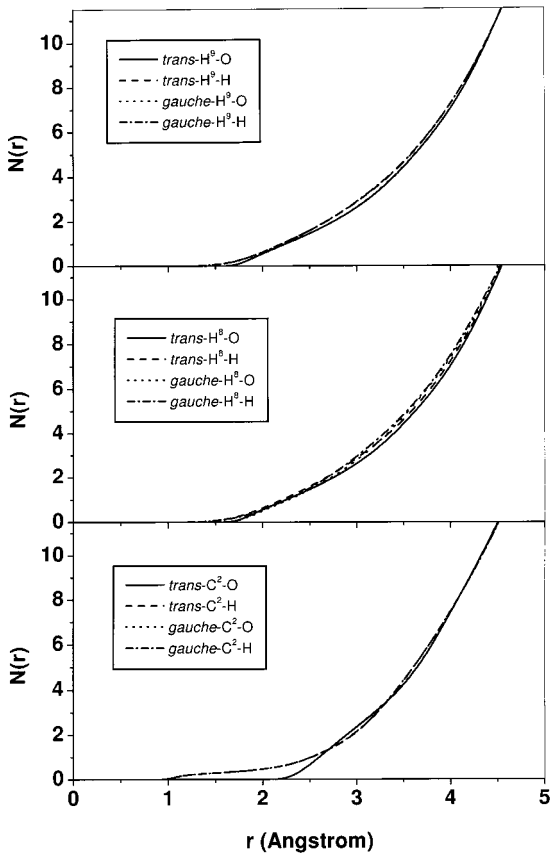

Figure 6. Running coordination numbers $N(r)$ for the *trans* and the *gauche* methylene group of *n*-butane in water.

distribution functions $g_{vv}(r)$ for pure water and their isothermal solute density derivative $\delta h_{vv}(r)$ with the scaling of $\rho_v/2$ for *n*-butane in water at infinite dilution. For comparison, in each figure we present our results for both the *trans* and the *gauche* conformers.

The comparison of the radial distribution functions of the *trans* and the *gauche* conformers shows that the *trans* conformer has slightly stronger effects on the water structure than the *gauche* conformer. This is because the *gauche* conformer has a more compact structure than the *trans* conformer. For both conformers, $\delta h_{vv}(r)$ have similar behavior as those of chloride ion and water solute molecule in water reported in the papers by Chong and Hirata[107] and Yu and Karplus,[65] i.e., they tend to distort and diminish the hydrogen bonding structure of water.

For comparison, we also did the same calculations with the united-atom OPLS model[108] and the all-atom OPLS model[16] for *n*-butane. The results corresponding to the united-atom OPLS model are shown in Figure 8. Comparing the corresponding curves in Figure 8 with Figure 7, one can see that $\delta h_{OO}(r)$ have similar behavior for both all-atom model and united-atom model, i.e., they tend to compress the peaks of $g_{OO}(r)$ inward and increase their heights; the negative through around 4.4 Å diminishes the tetrahedral coordination of the water oxygens. But $\delta h_{OH}(r)$ and $\delta h_{HH}(r)$ have different behavior for different solute models. With the united-atom model, $\delta h_{OH}(r)$ has dual effects (increase and decrease) on the hydrogen bonding peak of $g_{OH}(r)$. Remarkably, the heights of the two opposite sharp peaks are nearly equal to each other (0.69 for the positive peak and −0.70 for the negative peak) so the net effect of the $\delta h_{OH}(r)$ on the hydrogen bonding peak of $g_{OH}(r)$ is almost zero (see Figure 8b). With the united-atom model, $\delta h_{HH}(r)$ does not have the negative peak around the position of the first peak of $g_{HH}(r)$ and it strongly increases the first peak of $g_{HH}(r)$ (see Figure 8c). With the all-atom OPLS model, the corresponding curves are very similar to those in Figure 8. But all the positive peaks are slightly decreased. Significantly, in $\delta h_{OH}(r)$, the positive sharp peak is smaller than the negative one so that the net effect of the $\delta h_{OH}(r)$ is to decrease the hydrogen bonding peak.

Such results are typical to the RISM calculation in the (*N*, *V*, *T*) ensemble and reflect the effect of increased pressure disrupting the hydrogen bonding between water molecules. The all-atom model seems to enhance the effect of the disrupture of the water hydrogen bonding due to the well-documented shortcoming of the RISM theory in the treatment of the excluded volume of so-called auxiliary sites."[116] Experiments,[117−119] simulations,[120] and RISM calculations[121] all show that increased pressure causes disrupture of hydrogen bonding between water molecules.

$\delta h_{vv}(r)$ are related to the solute−solvent radial distribution functions $g_{CH}(r)$ through eq 4. We have seen that, with the all-atom model, the shortcomings in the HNC−RISM theory may cause unanticipated sharp peaks in $g_{C^1H}(r)$ and $g_{C^2H}(r)$, which in turn may cause enhancement of the negative peak in the $\delta h_{OH}(r)$.

The different behavior of the $\delta h_{vv}(r)$ with different all-atom models, our all-atom model vs the OPLS all-atom model, reflects the dependence of $\delta h_{vv}(r)$ on the Lennard-Jones parameter σ. Chong and Hirata[107] have shown that $\delta h_{vv}(r)$ are sensitive to the solute−solvent potential parameters, especially to σ. In particular, they showed that all the positive peaks in $\delta h_{vv}(r)$ are rapidly decreased with decreasing σ of the potassium ion. Notice that the corresponding site charges between our model and the all-atom OPLS model for *n*-butane are very close but the σ's in our model are much smaller. Therefore, with our all-atom model, all the positive peaks in $\delta h_{vv}(r)$ are much smaller than those obtained with the all-atom OPLS model and the positive sharp peak in $\delta h_{OH}(r)$ completely disappeared.

Further work on these issues are necessary by means of computer simulations with all-atom models.

C. Molecular Conformational Equilibria and Solvation Thermodynamics. In Figure 9 is shown the normalized equilibrium distribution of *n*-butane conformers $S(\phi)$ in ideal gas and aqueous phases and the solvent-induced rotational free energy surface $W_c(\phi)$. The qualitative features of our $S(\phi)$ and $W_c(\phi)$ are in rather good agreement with those obtained by means of experiments,[2,3,5,6] simulations[23,26−29] and other integral equation theories.[15,24] It can be seen that water is to lower the gas-phase rotational potential energies of the *cis* and *gauche* conformations relative to the *trans* conformation. There are mainly two conformations present in the gas and aqueous phases. One is the *gauche* conformation ($\phi = \pi/3$ and $5\pi/3$). The other one is the *trans* conformation ($\phi = \pi$). In the gas phase, the *trans* comformation is dominant. But in the aqueous phase the *gauche* conformation becomes dominant. There is a large shift from the *trans* conformation to the *gauche* conformation for the *n*-butane in the aqueous phase.

Quantitative comparison can be made by calculating the conformational equilibrium constant *K* and the *trans*−*cis* and *trans*−*gauche* cavity thermodynamic properties. In Table 5 are shown the equilibrium constants *K* at 25 °C for the *trans*−*gauche* isomerization of *n*-butane in gaseous and aqueous phases given by us and other authors. We obtain $K = 2.08$ in the aqueous phase, which is very close to Rosenberg et al.'s Monte Carlo simulation result[27] ($K = 2.3$). Comparing with Zichi and Rossky's united-atom HNC−RISM result[15] ($K \sim 4$),

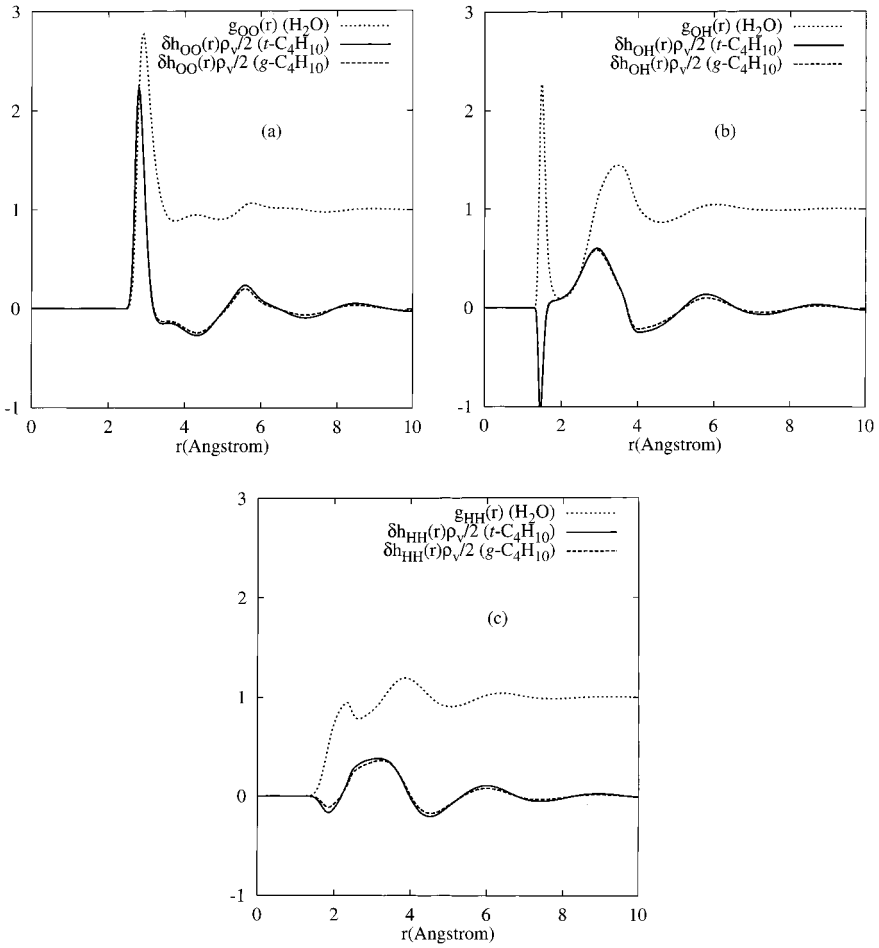

Figure 7. Radial distribution function $g_{vv}(r)$ for pure water and the corresponding isothermal solute density derivative $\delta h_{vv}(r)$ induced by *n*-butane in the all-atom representation at $T = 298.15$ K and $\rho_v = 0.03333$ molecules/Å^3. $\delta h_{vv}(r)$ is scaled by $\rho_v/2$. *t* for the *trans* conformer. *g* for the *gauche* conformer. (a) $g_{OO}(r)$ and $\delta h_{OO}(r)$ for water oxygen−water oxygen; (b) $g_{OH}(r)$ and $\delta h_{OH}(r)$ for water oxygen-water hydrogen; (c) $g_{HH}(r)$ and $\delta h_{HH}(r)$ for water hydrogen−water hydrogen.

TABLE 5: Equilibrium Constants at 25 °C for the *trans*−*gauche* Isomerization of *n*-Butane

	$K = x_g/x_t$	
authors	gas phase	H_2O
Pratt and Chandler[a]	0.50	1.2
Jorgensen[b]	0.47	1.0
Rosenberg et al.[c]	0.54	2.3
Zichi and Rossky[d]	0.54	∼4[e]
Jorgensen and Buckner[f]	0.47	0.79
Tobias and Brooks, united-atom[g]	0.54	0.54
Tobias and Brooks, all-atom[g]	0.59	0.85
exptl[h]	0.40−0.50	
this work	0.54	2.08

[a] Reference 24. [b] Reference 26. [c] Reference 27. [d] Reference 15. [e] Reference 23, estimated from Figure 2 of ref 15. [f] Reference 28. [g] Reference 23. [h] References 2, 3, 5, and 6.

one can see that our all-atom HNC−RISM computations predict a better *K*. But overall integral equation theories overestimate *K* in comparison with simulations. It also can be seen that with the united-atom model of butane, Tobias and Brooks, III, were unable to predict the change of *K* from the gas to the aqueous phase.

In Table 6 are shown the cavity thermodynamic properties calculated by us and other authors. The quantitative features of $W_c(\phi)$ can be measured by the *trans*−*cis* and *trans*−*gauche* cavity free energy $W_c(0)$ and $W_c(\pi/3)$. Overall, integral equation theories overestimate solvent effects on *n*-butane conformational change in comparison with simulations. But comparing with Zichi and Rossky's data, our $W_c(0)$ and $W_c(\pi/3)$ are in better agreement with the simulation results. All methods predict positive *trans*−*gauche* cavity entropy S_c which indicates that water is less ordered around the *gauche* conformer than around the *trans* conformer. This is consistent with the above solvation structural analysis in terms of the solute−solvent radial distribution functions. However, the RISM theory predicts the negative *trans*−*gauche* cavity energy E_c, while the simulation predicts the positive value.

Our calculated *n*-butane conformational average hydration thermodynamic properties: $\Delta\mu$, $\Delta\epsilon$, $T\Delta s$, Δh, and $T\Delta s_P$ at four thermodynamic states are listed in Table 7. The experimental data[60,61] are listed in parentheses. Our results show that around room temperature, *n*-butane has a large positive hydration free energy and a large negative hydration entropy. With increasing temperature, the hydration enthalpy and energy are increased. This will give a large positive heat capacity of hydration. Those features are consistent with the widely held view of thermodynamics of hydrophobic hydration and agree with experiments. Also, it can be seen that the entropy contribution to the hydration free energy is always larger than the energy contribution. *n*-butane hydration is thus an entropy-controlled process in agreement with experiments.

Inspection of Table 7 also shows that with the optimized CHARMM96 all-atom model, the prediction for the *n*-butane hydration thermodynamic properties by the HNC−RISM theory

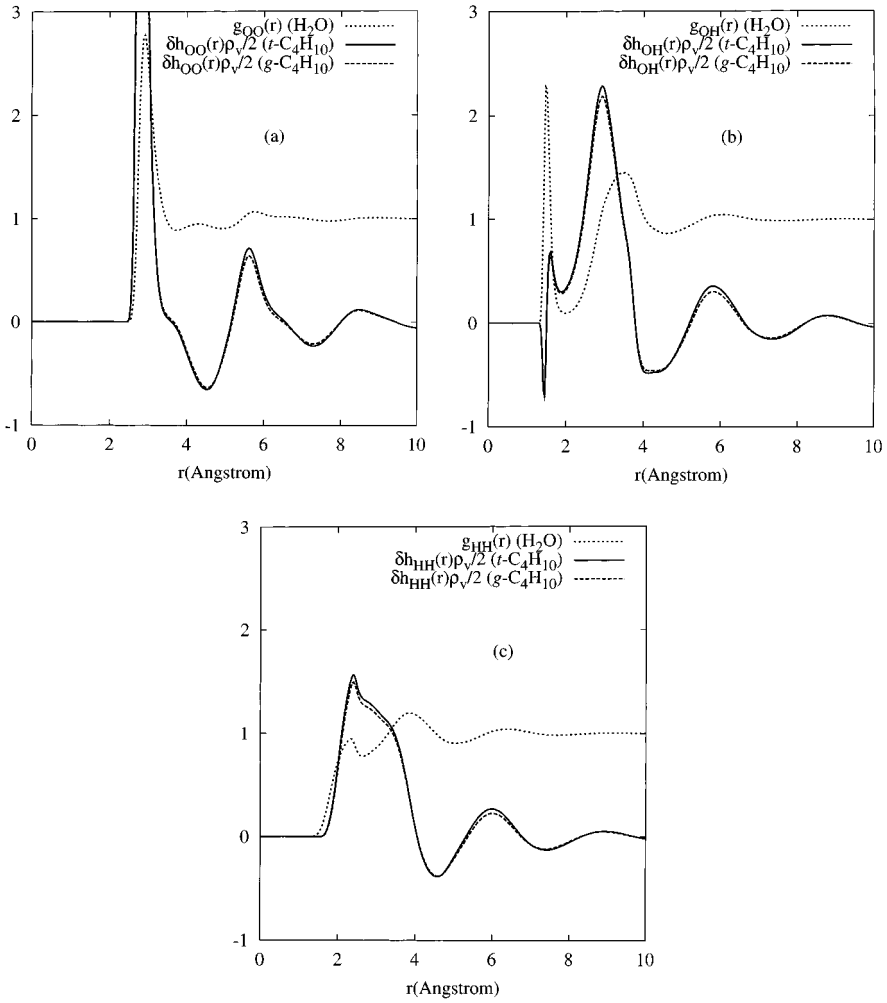

Figure 8. Same as Figure 7, except that united-atom OPLS model is employed for *n*-butane.

TABLE 6: Cavity Thermodynamics of *n*-Butane in Water at 25 °C in kcal/mol

model	$W_c(0)$	$W_c(\pi/3)$	$E_c(\pi/3)$	$-TS_c(\pi/3)$
Jorgensen[a]	−0.9	−0.5		
Jorgensen and Buckner[b]	−0.5	−0.3		
Beglov and Roux[c]	−0.5	∼ −0.2		
Tobias and Brooks, united-atom[d]		0.08 ± 0.02	2.74 ± 2.0	−2.66 ± 2.0
Tobias and Brooks, all-atom[d]		−0.17 ± 0.02	2.79 ± 2.7	−2.96 ± 2.7
Zichi and Rossky[e]	∼ −1.8	∼ −1.3	∼ −1.0	∼ −0.3
this work	−1.543	−0.855	−0.621	−0.234

[a] Reference 26. [b] Reference 28. [c] Estimated from Figure 8 of ref 29. [d] Reference 23. [e] Reference 23, estimated from the results and discussion of ref 15.

TABLE 7: *n*-Butane Hydration Free Energy $\Delta\mu$, Energy $\Delta\epsilon$, Entropy $T\Delta s$, Enthalpy Δh, and Entropy $T\Delta s_P$ in kcal/mol

T/K	ρ_{H_2O}/g cm^{-3} [a]	$\Delta\mu$	$-\Delta\epsilon$	$-T\Delta$s	$-\Delta$h	$-T\Delta s_P$
283.15	0.9997	1.345 (1.658)[b]	13.209	14.554	12.985 (6.994)	14.329 (8.653)
298.15	0.9970	2.034 (2.082)	12.756	14.790	12.024 (5.659)	14.058 (7.743)
313.15	0.9922	2.638 (2.439)	12.447	15.085	11.263 (4.322)	13.901 (6.761)
328.15	0.9875	3.166 (2.731)	12.178	15.344	10.589 (2.985)	13.755 (5.716)

[a] Reference 112. [b] Values in the parentheses are experimental values taken from refs 60 and 61.

are much improved. The rather good agreement between the theory and the experiment for the hydration free energies are obtained in all the temperature range of interest. But our predicted hydration enthalpies and hydration entropies are all overestimated and only qualitatively in agreement with the experimental data, even though the overestimations are much reduced by using the appropriate all-atom solute model. Noticing the shortcomings of the HNC−RISM theory, we believe that further correction can be made by using a more accurate closure other than HNC.

IV. Concluding Remarks

The solvation structure, solvation thermodynamics, and the molecular conformational equilibria for *n*-butane in water are analyzed by means of the HNC−RISM theory with the all-atom solute model.

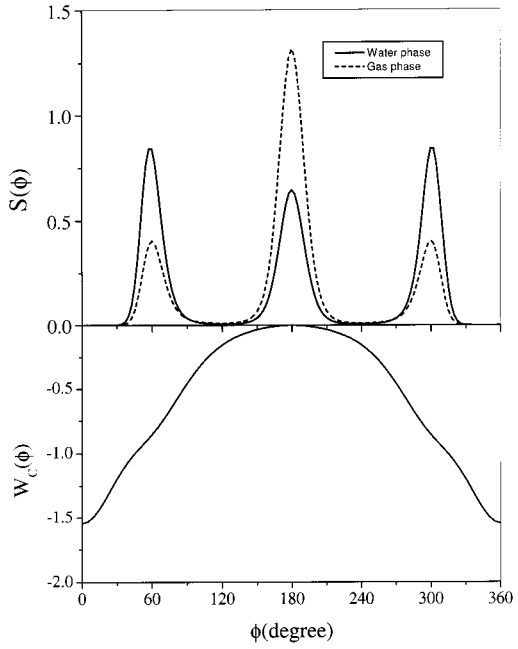

Figure 9. Normalized equilibrium distribution of conformers $S(\phi)$ and solvent-induced rotational free energy surface $W_c(\phi)$, in kcal/mol, for *n*-butane in water and ideal gas phases.

The solvation structure for the *trans* and the *gauche* conformers in water are presented and analyzed at the atomic level in terms of the atomic solute−solvent radial distribution functions. Our results show that water is more structured around the *trans* conformer than around the *gauche* conformer. For a fixed conformer, water is more structured around the methyl carbons than around the methylene carbons.

With the optimized CHARMM96 all-atom model, the *n*-butane hydration thermodynamic properties and its molecular conformational equilibria in water are well described by the HNC−RISM theory. Our predicted hydration free energies are in rather good agreement with experiments in all the temperature range of interest (10−55 °C). Qualitatively, our calculated $S(\phi)$ and $W_c(\phi)$ are in rather good agreement with computer simulations and experiments. There are mainly two conformations: *gauche* and *trans*, present in the gas and aqueous phases. The aqueous environment strongly favors the *gauche* conformation. Quantitatively, integral equation theories generally overestimate the *trans*−*gauche* equilibrium constant *K* and the *trans*−*cis* and the *trans*−*gauche* cavity free energies. However, our results are in better agreement with computer simulations than Zichi and Rossky's RISM calculations with the united-atom solute model.

We also calculated the solute density derivatives of the water−water radial distributaion functions, δh_{vv}, with the optimized CHARMM96 all-atom model, the united-atom OPLS and the all-atom OPLS models for *n*-butane, respectively. The $\delta h_{vv}(r)$ reflect the effect of increased pressure disrupting the hydrogen bonding between water molecules. The all-atom model seems to enhance such effect due to the well-documented shortcoming of the RISM theory in the treatment of the excluded volume of so-called auxiliary sites. Further work on this issue is necessary by means of computer simulations with all-atom models.

Acknowledgment. This research was supported in part by the Natural Sciences and Engineering Research Council of Canada (NSERC). We wish to thank Drs. F. Hirata, K. A. Dill, and N. T. Southall for helpful correspondence.

References and Notes

(1) Flory, P. J. *Statistical Mechanics of Chain Molecules*; Interscience: New York, 1969.
(2) Bartell, L. S.; Kohl, D. A. *J. Chem. Phys.* **1963**, *39*, 3097.
(3) Verma, A. L.; Murphy, W. F.; Bernstein, H. J. *J. Chem. Phys.* **1974**, *60*, 1540.
(4) Bradford, W. F.; Fitzwater, S.; Bartell, L. S. *J. Mol. Struct.* **1977**, *38*, 185.
(5) Durig, J. R.; Compton, D. A. *J. Phys. Chem.* **1979**, *83*, 265.
(6) Compton, D. A. C.; Montero, S.; Murphy, W. F. *J. Phys. Chem.* **1980**, *84*, 3587.
(7) Bell, C. D.; Harvey, S. C. *J. Phys. Chem.* **1986**, *90*, 6595.
(8) Tobias, D. J.; Brooks, C. L., III *J. Chem. Phys.* **1988**, *89*, 5115.
(9) Ryckaert, J. P.; Bellemans, A. *Chem. Phys. Lett.* **1975**, *30*, 123.
(10) Hsu, C. S.; Pratt, L. R.; Chandler, D. *J. Chem. Phys.* **1978**, *68*, 4213.
(11) Kint, S.; Scherer, J.; Snyder, R. G. *J. Chem. Phys.* **1980**, *73*, 2599.
(12) Snyder, J. R.; Snyder, R. G. *J. Chem. Phys.* **1980**, *72*, 5798.
(13) Colombo, L.; Zerbi, G. *J. Chem. Phys.* **1980**, *73*, 2013.
(14) Jorgensen, W. L. *J. Phys. Chem.* **1983**, *87*, 5304.
(15) Zichi, D. A.; Rossky, P. J. *J. Chem. Phys.* **1986**, *84*, 1712.
(16) Kaminski, G.; Duffy, E. M.; Matsui, T.; Jorgensen, W. L. *J. Phys. Chem.* **1994**, *98*, 13077.
(17) Jorgensen, W. L.; Maxwell, D. S.; Tirado-Rives, J. *J. Am. Chem. Soc.* **1996**, *118*, 11225.
(18) Pratt, L. R.; Hsu, C. S.; Chandler, D. *J. Chem. Phys.* **1978**, *68*, 4202.
(19) Rebertus, D. W.; Berne, B. J.; Chandler, D. *J. Chem. Phys.* **1979**, *70*, 3395.
(20) Pratt, L. R.; Rosenberg, R. O.; Berne, B. J.; Chandler, D. *J. Chem. Phys.* **1980**, *73*, 1002.
(21) Bigot, B.; Jorgensen, W. L. *J. Chem. Phys.* **1981**, *75*, 1944.
(22) Rosenthal, L.; Rabolt, J. F.; Hummel, J. *J. Chem. Phys.* **1982**, *76*, 817.
(23) Tobias, D. J.; Brooks, C. L., III *J. Chem. Phys.* **1990**, *92*, 2582.
(24) Pratt, L. R.; Chandler, D. *J. Chem. Phys.* **1977**, *67*, 3683.
(25) Pratt, L. R.; Chandler, D. *J. Chem. Phys.* **1980**, *73*, 3430.
(26) Jorgensen, W. L. *J. Chem. Phys.* **1982**, *77*, 5757.
(27) Rosenberg, R. O.; Mikkilineni, R.; Berne, B. J. *J. Am. Chem. Soc.* **1982**, *104*, 7647.
(28) Jorgensen, W. L.; Buckner, J. K. *J. Phys. Chem.* **1987**, *91*, 6083.
(29) Beglov, D.; Roux, B. *J. Chem. Phys.* **1994**, *100*, 9050.
(30) Hummer, G.; Garde, S.; Garcia, A. E.; Pohorille, A.; Pratt, L. R. *Proc. Natl. Acad. Sci. U.S.A.* **1996**, *93*, 8951.
(31) Hummer, G.; Garde, S.; Garcia, A. E.; Paulaitis, M. E.; Pratt, L. R. *J. Phys. Chem. B* **1998**, *102*, 10469.
(32) Du, Q.; Beglov, D.; Roux, B. *J. Phys. Chem. B* **2000**, *104*, 796.
(33) Kovalenko, A.; Hirata, F. *J. Chem. Phys.* **2000**, *113*, 2793.
(34) Chandler, D.; Andersen, H. C. *J. Chem. Phys.* **1972**, *57*, 1930.
(35) Lowden, L. J.; Chandler, D. *J. Chem. Phys.* **1974**, *61*, 5228.
(36) Hirata, F.; Pettitt, B. M.; Rossky, P. J. *J. Chem. Phys.* **1982**, *77*, 509.
(37) Pettitt, B. M.; Rossky, P. J. *J. Chem. Phys.* **1982**, *77*, 1451.
(38) Hirata, F.; Rossky, P. J.; Pettitt, B. M. *J. Chem. Phys.* **1983**, *78*, 4133.
(39) Hirata, F. *Bull. Chem. Soc. Jpn.* **1998**, *71*, 1438.
(40) Ichiye, T.; Chandler, D. *J. Phys. Chem.* **1988**, *92*, 5257.
(41) Lue, L.; Blankschtein, D. *J. Phys. Chem.* **1992**, *96*, 8582.
(42) Kinoshita, M.; Hirata, F. *J. Chem. Phys.* **1997**, *106*, 5202.
(43) Perkyns, J. S.; Pettitt, B. M. *J. Phys. Chem.* **1996**, *100*, 1323.
(44) Kovalenko, A.; Truong, T. N. *J. Chem. Phys.* **2000**, *113*, 7458.
(45) Hansen, J. P.; McDonald, I. R. *Theory of Simple Liquids*; Academic: London, 1976.
(46) Hsu, C. S.; Chandler, D.; Lowden, L. J. *Chem. Phys.* **1976**, *14*, 213.
(47) Cummings, P. T.; Gray, C. G.; Sullivan, D. E. *J. Phys. A* **1981**, *14*, 1483.
(48) Martynov, G. A.; Sarkisov, G. N. *Mol. Phys.* **1984**, *49*, 1495.
(49) Ballone, P.; Pastore, G.; Galli, G.; Gazzillo, D. *Mol. Phys.* **1986**, *59*, 275.
(50) Beglov, D.; Roux, B. *J. Phys. Chem. B* **1997**, *101*, 7821.
(51) Chandler, D.; McCoy, J. D.; Singer, S. J. *J. Chem. Phys.* **1986**, *85*, 5971.
(52) Kovalenko, A.; Hirata, F. *Chem. Phys. Lett.* **1998**, *290*, 237.
(53) Kovalenko, A.; Ten-no, S.; Hirata, F. *J. Comput. Chem.* **1999**, *20*, 928.
(54) Kovalenko, A.; Hirata, F. *J. Chem. Phys.* **1999**, *110*, 10095.
(55) Kovalenko, A.; Hirata, F. *J. Phys. Chem. B* **1999**, *103*, 7942.
(56) Kovalenko, A.; Hirata, F. *J. Chem. Phys.* **2000**, *112*, 10391.
(57) Cui, Q.; Smith, V. H., Jr. *J. Chem. Phys.* **2000**, *113*, 10240.
(58) Cui, Q.; Smith, V. H., Jr. *J. Chem. Phys.* **2001**, *115*, 2228.
(59) Yin, D.; Mackerell, A. D., Jr. *J. Comput. Chem.* **1998**, *19*, 334.

(60) Wilhelm, E.; Battino, R.; Wilcock, R. J. *Chem. Rev.* **1977**, *77*, 219.
(61) Ben-Naim, A.; Marcus, Y. *J. Chem. Phys.* **1984**, *81*, 2016.
(62) Bowron, D. T.; Filipponi, A.; Roberts, M. A.; Finney, J. L. *Phys. Rev. Lett.* **1998**, *81*, 4164.
(63) Southall, N. T.; Dill, K.; Haymet, A. D. J. *J. Phys. Chem. B* **2002**, *106*, 521.
(64) Frank, H. S.; Evans, M. W. *J. Chem. Phys.* **1945**, *13*, 507.
(65) Yu, H.-A.; Karplus, M. *J. Chem. Phys.* **1988**, *89*, 2366.
(66) Shinoda, K. *J. Phys. Chem.* **1977**, *81*, 1300.
(67) Tanaka, H. *J. Chem. Phys.* **1987**, *86*, 1512.
(68) Owicki, J. C.; Scheraga, H. A. *J. Am. Chem. Soc.* **1977**, *99*, 7413.
(69) Swaminathan, S.; Harrison, S. W.; Beveridge, D. L. *J. Am. Chem. Soc.* **1978**, *100*, 5705.
(70) Geiger, A.; Rahman, A.; Stillinger, F. H. *J. Chem. Phys.* **1979**, *70*, 263.
(71) Rossky, P. J.; Karplus, M. *J. Am. Chem. Soc.* **1979**, *101*, 1913.
(72) Okazaki, S.; Nakanishi, K.; Touhara, H.; Adachi, Y. *J. Chem. Phys.* **1979**, *71*, 2421.
(73) Okazaki, S.; Nakanishi, K.; Touhara, H.; Watanabe, N.; Adachi, Y. *J. Chem. Phys.* **1981**, *74*, 5863.
(74) Mezei, M.; Beveridge, D. L. *J. Chem. Phys.* **1981**, *74*, 622.
(75) Rapaport, D. C.; Scheraga, H. A. *J. Phys. Chem.* **1982**, *86*, 873.
(76) Tanaka, H.; Nakanishi, K. *J. Chem. Phys.* **1991**, *95*, 3719.
(77) Matubayasi, N. *J. Am. Chem. Soc.* **1994**, *116*, 1450.
(78) Madan, B.; Sharp, K. A. *J. Phys. Chem.* **1996**, *100*, 7713.
(79) Sharp, K. A.; Madan, B. *J. Phys. Chem. B* **1997**, *101*, 4343.
(80) Ikeguchi, M.; Shimizu, S.; Nakamura, S.; Shimizu, K. *J. Phys. Chem. B* **1998**, *102*, 5891.
(81) Sharp, K. A.; Madan, B.; Manas, E.; Vanderkooi, J. M. *J. Chem. Phys.* **2001**, *114*, 1791.
(82) Filipponi, A.; Bowron, D. T.; Lobban, C.; Finney, J. L. *Phys. Rev. Lett.* **1997**, *79*, 1293.
(83) deJone, P. H. K.; Wilson, J. E.; Neilson, G. W.; Buckingham, A. D. *Mol. Phys.* **1997**, *91*, 99.
(84) Mizuno, K.; Miyashita, Y.; Shindo, Y.; Ogawa, H. *J. Phys. Chem.* **1995**, *99*, 3225.
(85) Lum, K.; Chandler, D.; Weeks, J. D. *J. Phys. Chem. B* **1999**, *103*, 4570.
(86) ten Wolde, P. R.; Sun, S. X.; Chandler, D. *Phys. Rev. E* **2001**, *65*, 011201.
(87) Silverstein, K. A. T.; Dill, K. A.; Haymet, A. D. J. *J. Chem. Phys.* **2001**, *114*, 6303.
(88) Huang, D. M.; Chandler, D. *J. Phys. Chem. B* **2002**, *106*, 2047.
(89) Ashbaugh, H. S.; Truskett, T. M.; Debenedetti, P. G. *J. Chem. Phys.* **2002**, *116*, 2907.
(90) Lee, C. Y.; McCammon, J. A.; Rossky, P. J. *J. Chem. Phys.* **1984**, *80*, 4448.
(91) Guillot, B.; Guissani, Y.; Bratos, S. *J. Chem. Phys.* **1991**, *95*, 3643.
(92) Guillot, B.; Guissani, Y. *J. Chem. Phys.* **1993**, *99*, 8075.
(93) Lazaridis, T.; Paulaitis, M. E. *J. Phys. Chem.* **1994**, *98*, 635.
(94) Beutler, T. C.; Béguelin, D. R.; van Gunsteren, W. F. *J. Chem. Phys.* **1995**, *102*, 3787.
(95) Wallqvist, A.; Berne, B. J. *J. Phys. Chem.* **1995**, *99*, 2885.
(96) Mancera, R. L.; Buckingham, A. D. *J. Phys. Chem.* **1995**, *99*, 14632.
(97) Chau, P. L.; Forester, T. R.; Smith, W. *Mol. Phys.* **1996**, *89*, 1033.
(98) Lynden-Bell, R. M.; Rasaiah, J. C. *J. Chem. Phys.* **1997**, *107*, 1981.
(99) Floris, F. M.; Selmi, M.; Tani, A.; Tomasi, J. *J. Chem. Phys.* **1997**, *107*, 6353.
(100) Arthur, J. W.; Haymet, A. D. J. *J. Chem. Phys.* **1998**, *109*, 7991.
(101) Cheng, Y.; Rossky, P. J. *Nature* **1998**, *392*, 696.
(102) Cheng, Y.; Sheu, W.; Rossky, P. J. *Biophys. J.* **1999**, *76*, 1734.
(103) Southall, N. T.; Dill, K. *J. Phys. Chem. B* **2000**, *104*, 1326.
(104) Urbič, T.; Vlachy, V.; Kalyuzhnyi, Y. V.; Southall, N. T.; Dill, K. A. *J. Chem. Phys.* **2002**, *116*, 723.
(105) Du, Q.; Freysz, E.; Shen, Y. R. *Science* **1994**, *264*, 826.
(106) Silverstein, K. A. T.; Haymet, A. D. J.; Dill, K. A. *J. Am. Chem. Soc.* **1998**, *120*, 3166.
(107) Chong, S. H.; Hirata, F. *J. Phys. Chem. B* **1997**, *101*, 3209.
(108) Jorgensen, W. L.; Madura, J. D.; Swenson, C. J. *J. Am. Chem. Soc.* **1984**, *106*, 6638.
(109) Singer, S. J.; Chandler, D. *Mol. Phys.* **1985**, *55*, 621.
(110) Yu, H.-A.; Roux, B.; Karplus, M. *J. Chem. Phys.* **1990**, *92*, 5020.
(111) McQuarrie, D. A. *Statistical Mechanics*; Harper and Row*:* New York, 1976.
(112) *Handbook of Chemistry and Physics*, 67th ed.; Weast, R. C., Ed.; CRC Press: Boca Raton, FL, 1986/1987.
(113) Chandler, D. *in The Liquid State of Matter: Fluids, Simple and Complex*; Montroll, E. W., J. L. Lebowitz, J. L., Eds.; North-Holland, New York, 1982.
(114) Chandler, D. *Faraday Discuss. Chem. Soc.* **1978**, *66*, 184.
(115) Jorgensen, W. L.; Chandrasekhar, J.; Madura, J. D.; Impey, R. W.; Klein, M. L. *J. Chem. Phys.* **1983**, *79*, 926.
(116) Hirata, F. Private communications.
(117) Horne, R. A.; Hohnson, D. S. *J. Phys. Chem.* **1966**, *70*, 2182.
(118) Wu, A. Y.; Whalley, E.; Dolling, C. *Chem. Phys. Lett.* **1981**, *84*, 433.
(119) Polo, J. A.; Egelstaff, P. A. *Phys. Rev. A* **1983**, *27*, 1508.
(120) Impey, R. W.; Klein, M. L.; McDonald, I. R. *J. Chem. Phys.* **1981**, *74*, 647.
(121) Pettitt, B. M.; Calef, D. F. *J. Phys. Chem.* **1987**, *91*, 1541.
(122) Weiner, S. J.; Kollman, P. A.; Nguyen, D. T.; Case, D. A. *J. Comput. Chem.* **1986**, *7*, 230.